Available online at www.sciencedirect.com
SCIENCE DIRECT
Journal of Molecular Catalysis A: Chemical 252 (2006) 202–211
JOURNAL OF MOLECULAR CATALYSIS A: CHEMICAL
www.elsevier.com/locate/molcata

NO_2-catalyzed deep oxidation of methanol: Experimental and theoretical studies

Chao-Xian Xiao [a], Ning Yan [a], Ming Zou [a], Si-Cong Hou [a], Yuan Kou [a,*], Wenjian Liu [a,*], Shaowen Zhang [b]

[a] *College of Chemistry and Molecular Engineering, Peking University, Beijing 100871, PR China*
[b] *College of Science, Beijing Institute of Technology, Beijing 100081, PR China*

Received 31 May 2005; received in revised form 17 February 2006; accepted 23 February 2006
Available online 3 April 2006

Abstract

The NO_2-catalyzed deep oxidation of methanol has been studied by both experimental and theoretical techniques. On-line infrared (IR) and in situ IR investigations show that a trace amount of NO_x (for example, 600 ppm NO and/or NO_2) can dramatically promote the oxidation of methanol as manifested by the reduced reaction temperature together with significantly enhanced CO_2 selectivity. The reactions of methanol and nitrogen dioxide are investigated by theoretical calculations at the CBS-Q//B3LYP/6-311++G(2d,p) level of theory. Seven channels are found totally. The calculated reaction barriers of the controlling steps of the two lowest channels are 20.5 and 21.1 kcal mol^{-1}, which are in good agreement with the reported experimental value of 21.4 kcal mol^{-1}. The reaction rate constants are also calculated by the microcanonical variational transition state theory (μVT) with tunneling corrections. The three-parameter fitting expression for the overall forward rate constant is $1.72 \times 10^{-22} T^{3.38} \exp(-10153\ T^{-1})$ cm^3 $molecule^{-1}$ s^{-1}. The theoretical simulation of methanol conversion is in satisfactory agreement with the experiment. A reaction mechanism for the CH_3OH–O_2–NO_x system has been proposed based on the experimental and theoretical studies.

Keywords: Methanol oxidation; Nitrogen dioxide; Catalysis; Modeling; Reaction mechanism

1. Introduction

Although the reactions involved in the CH_4–O_2–NO_x co-feed system have been comprehensively investigated [1–7], those in the related CH_3OH–O_2–NO_x system have not yet been so widely studied. The reactions in the latter system are related to at least three important areas, i.e., selective oxidation of methane to oxygenates including methanol [1–7], complete combustion of methanol as a gasoline additive [8], and selective reduction of NO by methane [9]. The three areas are relatively independent and are not routinely well cross-referenced in the literature.

The selective oxidation of methane promoted by NO_x (NO and/or NO_2) has been shown to give a variety of oxygenates (mainly methanol and formaldehyde) [1–7]. Methanol is the desired product in such a process but the yield is normally far from being satisfactory [1–4]. The best yield of oxygenates as reported by Tabata et al. [1] and Otsuka et al. [2] is lower than 7% at a temperature of 873 K with an NO_x concentration of 0.5%. Deep oxidation of methanol, which is more active than methane, is a key factor responsible for the low yield. What role NO_x plays in the deep oxidation still has not been clearly characterized, however. Understanding the mechanism, in particular, the mechanistic difference between the conversion of methane and methanol, is thus of great value in finding a process that can make selective oxidation of methane more feasible.

Methanol is nowadays considered as an alternative to gasoline for transport on environmental grounds. In combustion processes such as in automobile engines, NO_x is formed from thermal fixation of molecular nitrogen at high temperatures. The NO_x concentrations are typically 10–1000 ppm. Yano [8] has found that NO can considerably accelerate the oxidation of residual methanol to formaldehyde in the exhaust of methanol-fueled engines. Incomplete combustion of these oxygenates may cause further environmental problems. Furthermore, from a mechanis-

* Corresponding authors. Tel.: +86 10 62757792; fax: +86 10 62751708.
E-mail addresses: yuankou@pku.edu.cn (Y. Kou), liuwj@pku.edu.cn (W. Liu).

1381-1169/$ – see front matter © 2006 Elsevier B.V. All rights reserved.
doi:10.1016/j.molcata.2006.02.064

tic view of point, it is not clear whether or not NO_x reacts with alcohols stoichiometrically [10,11].

The catalytic reduction of NO_x to N_2 with methane is a potentially useful strategy for the remediation of exhaust from natural gas-fired power plants and lean-burn natural-gas engines [9]. However, methanol may be formed in this process via the intermediate CH_3NO as reported by Ying [9]. As mentioned above, even a low level of methanol in the exhaust may result in external environmental problems, and the formation of methanol should be avoided via deep oxidation.

It is worthwhile noting that NO_x-promoted gas phase oxidation of methanol has many advantages as far as performing in situ IR or theoretical studies are concerned. The absence of a solid catalyst, together with the high IR sensitivities of the different products, means that in situ observations can be carried out with either very low or very high methanol concentrations, over a very wide temperature range. In our previous paper [5], by comparison of the in situ IR spectra with the on-line results we have shown that the HONO species, which is observed only by in situ measurements, is a key intermediate in the NO_x-promoted gas-phase oxidation of methane. In this paper we report on-line reaction studies, in situ IR experiments, and theoretical calculations that allow us to conclude that deep oxidation of methanol to carbon oxides can be catalyzed by NO_2.

2. Experimental details

The procedure used a conventional gas flow reactor system. Three separate streams of NO/N_2 (1880 ppm NO, or 1.56% NO alternatively, N_2 balanced), O_2 (99.995%) and N_2 (99.999%) were used. Flow rates were adjusted by mass flow controllers. Three streams were premixed (typical composition: 600 ppm NO, 5% O_2 and 95% N_2, respectively) prior to being bubbled through liquid methanol (>99.5%, dipped in ice water). Then, the gas mixture flowed through a quartz tube (heating length 20 cm, i.d. 5.8 mm, flow rate 40 ml min^{-1}), which was heated at temperatures ranging from room temperature to 873 K. The exit mixture was analyzed by on-line FT-IR using a Bruker Vector 22 infrared spectrometer with a gas cell (length 10 cm, KBr widows). In the case of NO concentration measurement, the exit mixture flowed through a P_2O_5 drier prior to the quantitative analysis, in order to exclude the water interference. The concentrations of the products were computed automatically with the OPUS quantitative method using calibration curves. On-line mass spectrometer (HIDEN HPR-20 gas analyzer) was used to further check the low concentration compounds (NO_2, CH_3NO_2, etc.) in the exit mixture.

The in situ experiments were carried out in a homemade quartz infrared cell (i.d. 10 mm, length 15 cm). KBr windows cooled by flowing water were attached to both sides of the cell. A 7.5 cm heating element wrapped around the cell allowed collection of in situ spectra at elevated temperatures. The temperature was monitored by a thermocouple located on the outside of the cell (and near the heating element) and was calibrated by another thermocouple put in the cell under the same conditions. In situ infrared spectra were collected using a Bruker Vector 22 spectrometer with a resolution of 2 cm^{-1}.

3. Computational details

3.1. Electronic structure calculations

The electronic structure calculations were performed using the Gaussian 98 program package [12]. The geometries of all the stationary points were optimized by employing the hybrid density functional B3LYP method (Becke's three-parameter nonlocal exchange functional [13] with the correlation functional of Lee, Yang and Parr [14,15]) with the 6-311++G(2d,p) basis set. To obtain more accurate energies, the complete basis set method CBS-Q [16] was employed to refine the energies based on the geometries optimized at the B3LYP/6-311++G(2d,p) level of theory. All the transition states were confirmed by frequencies and IRC (intrinsic reaction coordinate) calculations with the B3LYP/6-311++G(2d,p) method. All the energies in this study were corrected with the ZPE (zero point energy) except those pointed out explicitly. The ZPE and frequencies were not scaled due to the use of triple-zeta basis sets.

3.2. Rate constant calculations

Within the framework of microcanonical variational transition state theory (μVT), the thermal rate constant at a given temperature T can be expressed as:

$$k^{\mu VT}(T) = \sigma \frac{\int_0^\infty \min_s \{N^{GTS}(E,s)\} e^{-E/k_B T} dE}{h Q_R}$$

where σ is the statistical factor of the reaction, and h and k_B are the Planck and Boltzman constants, respectively. Q_R is the total reactant partition function, which is the product of electronic, rotational and vibrational partition functions. The relative translational partition function was calculated classically. However, the rotational and vibrational partition functions of the reactant were calculated quantum mechanically within the rigid rotor and harmonic oscillator approximations. $N^{GTS}(E, s)$ is the sum of states of electronic, rotational and vibrational motions at energy E of the generalized transition state located at the reaction coordinate s. $N^{GTS}(E, s)$ along the minimum energy path were also calculated quantum mechanically using the rigid rotor and harmonic oscillator approximations. Since all the channels involve hydrogen transfer, the tunneling effects were calculated and included in $N^{GTS}(E, s)$ using the Eckart potential. The forward and reverse symmetry factors are 6 and 2 for channels 1–3, and 3 and 2 for channel 4, respectively. All the rate constant calculations were carried out with the VKLab 1.0 program [17].

4. Results and discussion

4.1. Spontaneous oxidation of methanol

The results of one pass oxidation of methanol in the absence of NO are shown in Table 1. It can be seen that the temperature required for initiating the spontaneous oxidation of methanol is at least 773 K.

Table 1
Summary of experimental results (1 bar, O_2 5%, N_2 balance, gas flow rate 40 ml min^{-1})

NO (ppm)	Temperature (K)	CH_3OH (%)	CO_2 (%)	CO (%)
None	298	4.24	None	None
None	673	4.18	None	None
None	723	4.06	None	None
None	773	3.41	Trace	0.04
None	823	2.73	Trace	0.11
None	873	2.56	Trace	0.10
600	298	4.23	None	None
600	673	3.91	None	Trace
600	723	3.78	Trace	Trace
600	773	3.27	0.02	0.11
600	823	2.24	0.10	0.21
600	873	0.58	3.41	1.09
10000	298	4.24	None	None
10000	623	3.80	Trace	None
10000	673	3.32	0.04	Trace
10000	773	1.70	2.01	0.42
10000	873	0.52	3.52	0.77

As shown in Table 1, the main products of the spontaneous oxidation are carbon oxides. However, a trace amount of methylal ($CH_3OCH_2OCH_3$) was also detected in the exit mixture by on-line IR (Fig. 1). It seems that methylal was formed through the following reaction [18,19]:

$$2CH_3OH + CH_2O \rightarrow CH_3OCH_2OCH_3 + H_2O \quad (1)$$

that is, the oxidation process begins with the partial oxidation of methanol to formaldehyde, and then formaldehyde undergoes deep oxidation to carbon oxides [28], as well as reacting with methanol to form methylal. Furthermore, Table 1 shows that increasing the reaction temperature may significantly enhance the conversion of methanol. At 873 K, at which temperature the activation of methane to oxygenates including methanol is normally observed, the conversion of methanol giving mainly carbon oxides increases to 40%, implying that the spontaneous gas-phase deep oxidation of methanol to carbon oxides is not negligible at this temperature.

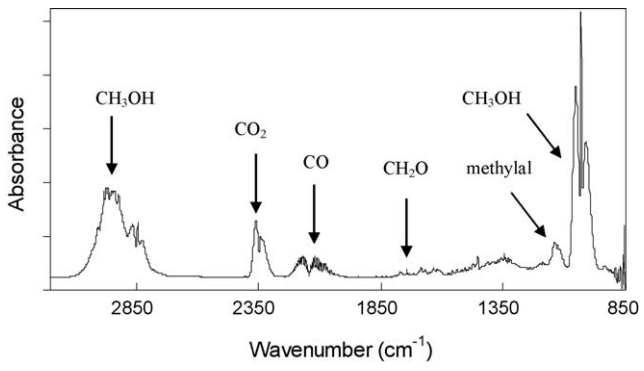

Fig. 1. IR spectrum of product mixture. Reaction conditions: CH_3OH 5%, O_2 5%, N_2 balance, flow rate 40 ml min^{-1}, 823 K.

4.2. NO_2-catalyzed oxidation

The catalytic role that NO_2 plays can be manifested by either a significantly reduced reaction temperature or a dramatically increased CO_2 selectivity under the conditions where the total concentration of NO and NO_2 remains unchanged. The concentration of NO in the exit mixture was measured by means of its IR absorption bands in the range 1820–1940 cm^{-1} (the water absoption bands in this range disappear after flowing through the P_2O_5 dyier), and that of NO_2 was simultaneously measured by on-line MS. It can be seen from Fig. 2 that the total concentration of NO and NO_2 (i.e., NO_x) do not change significantly over the reaction temperature range while the amount of NO_2 monitored by on-line MS is about 100 ppm. For example, when 600 ppm NO was present in the co-feed gases, more than 400 ppm NO remained while the rest seemed to be transformed to NO_2 following the chemical equilibrium between NO and NO_2:

$$2NO + O_2 \leftrightarrow 2NO_2 \quad (2)$$

CH_3NO_2 was also detected, but its concentration was only 5% of the feed NO (cf. Fig. 2).

Compared to 773 K in the absence of NO, the initiating temperature for the deep oxidation of methanol was only about 673 K in the presence of 600 ppm NO (cf. Table 1). The temperature can be further reduced to 623 K when the NO concentration was increased to 1%. The $T_{50\%}$ (defined as the temperature at which 50% of CH_3OH is converted) was at least higher than 873 K in the absence of NO, but was reduced to about 830 K (calculated based on the fitting curve shown in Fig. 3) in the presence of 600 ppm NO. The turnover frequency (TOF) [20] based on NO at a concentration of 600 ppm was estimated at approximately 4 s^{-1} at 873 K for the reaction.

It is clear that the oxidation of methanol is remarkably enhanced in the presence of NO, that is to say, the addition of NO changes the product distribution dramatically. In the presence of

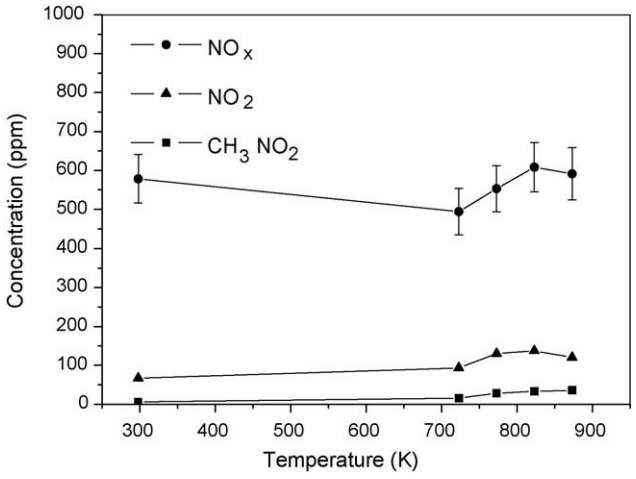

Fig. 2. The NO_x (NO and NO_2) and CH_3NO_2 concentrations after reaction at different temperatures. Reaction conditions: CH_3OH 5%, O_2 5%, N_2 balance, NO 600 ppm, flow rate 40 ml min^{-1}.

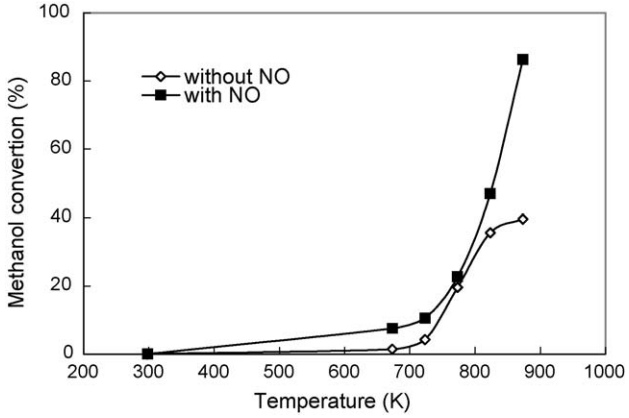

Fig. 3. The effects of NO on the oxidation of methanol at different temperatures. Reaction conditions: CH_3OH 5%, O_2 5%, N_2 balance, NO 600 ppm, flow rate 40 ml min^{-1}.

NO, the major product is carbon dioxide, while in the absence of NO, carbon monoxide is predominant (see Fig. 4 and Table 1). For example, it can be seen in Fig. 4 that the selectivity to CO_2 is about 76% at a temperature of 873 K in the presence of 600 ppm NO while it does not reach 10% at the same temperature in the absence of NO.

It is not clear whether it is NO or NO_2 that initiates the reaction since both NO and NO_2 are odd-electron species and are, in principle, capable of abstracting hydrogen atoms. To clarify this, NO_2 was introduced into the reaction instead of NO. The results are shown in Fig. 5. Carbon monoxide is observed at the very low temperature of 573 K in the presence of NO_2, implying NO_2 has much higher reactivity than NO. At higher temperatures (above 723 K), however, the performance of NO and NO_2 are virtually the same due to the fact that reaction (2) reaches its equilibrium immediately at higher temperatures.

These results strongly suggest that it should be NO_2, instead of NO, that plays a catalytic role in the deep oxidation of methanol. Thorough discussions on the reactions of CH_3OH and NO_2 will be given in Section 4.

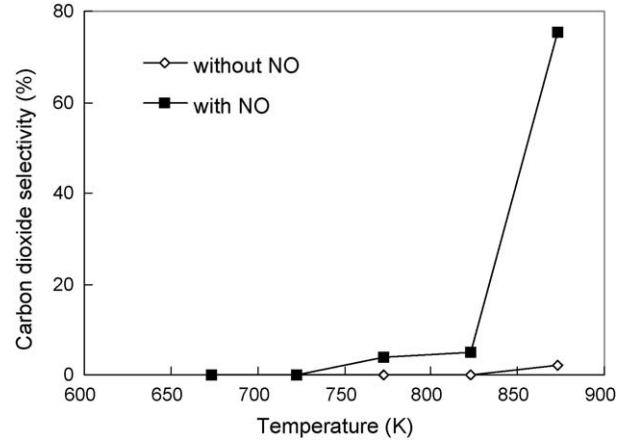

Fig. 4. The effects of NO on carbon dioxide at different temperatures. Reaction conditions: CH_3OH 5%, O_2 5%, N_2 balance, NO 600 ppm, flow rate 40 ml min^{-1}.

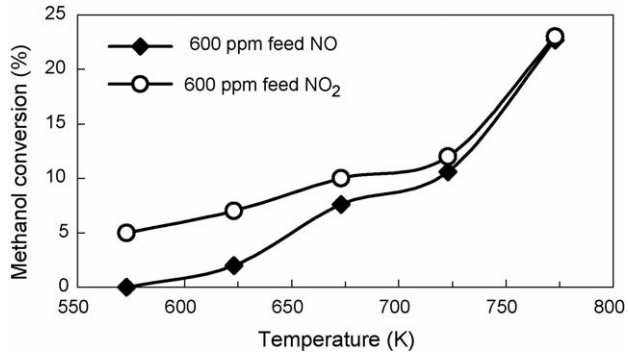

Fig. 5. Comparison of the effects of feed NO or NO_2 on methanol conversion at different temperatures. Reaction conditions: CH_3OH 5%, O_2 5%, NO (or NO_2) 600 ppm, N_2 balance, flow rate 40 ml min^{-1}.

4.3. In situ IR measurements

The in situ FT-IR investigation shows that the yield of each product in the CH_3OH–O_2–NO_x system varies significantly under different reaction conditions. The most important condition is reaction temperature. It can be seen from Fig. 6 that the formation of HCHO is observed at 733–753 K, and that then CO (753 K) and CO_2 (773 K) are observed. This result is in agreement with the methanol oxidation mechanism proposed by Westbrook and Dryer [28], HCHO is not detectable above 773 K. The yield of CO increases with temperature, and reaches a maximum at a temperature of 773–793 K.

The in situ infrared spectra have been carefully compared with the on-line results. The absorption bands due to the main products (CO_2, CO and HCHO) observed in situ are consistent with those obtained on-line. However, it is noteworthy that the absorption of methylal ($CH_3OCH_2OCH_3$) can only be observed on-line, further suggesting that methylal is formed through reaction (1) under lower temperatures after the oxidation reaction zone. On the other hand, weak HONO absorption bands, which are absent in the on-line spectra, are observed in the 1000–700 cm^{-1} region of the in situ spectra (Fig. 7) when

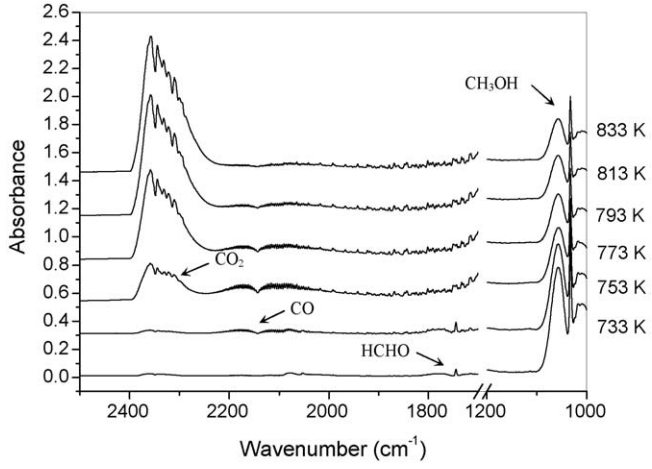

Fig. 6. The in situ product distributions in the CH_3OH–O_2–NO_x system at different temperatures. Reaction conditions: CH_3OH 4%, O_2 20%, NO 600 ppm, N_2 balance, flow rate 80 ml min^{-1}.

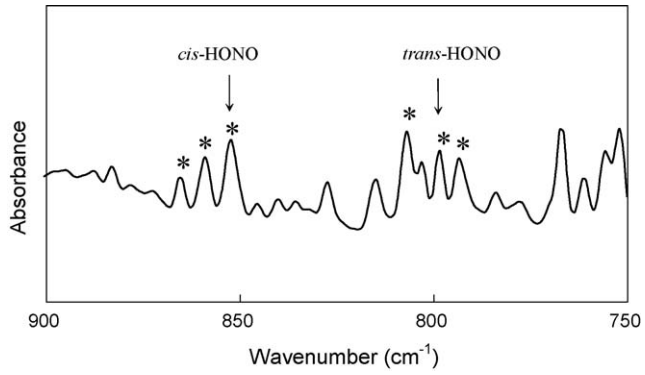

Fig. 7. HONO absorption in the in situ IR spectrum. For the assignment of *cis*-HONO and *trans*-HONO see ref. [5]. The asterisks indicate the NO stretching vibrations of HONO. Reaction conditions: CH_3OH 4%, O_2 20%, NO 600 ppm, N_2 balance, flow rate 80 ml min^{-1}, 793 K.

the reaction is initiated. HONO is believed to be an important intermediate in the catalytic cycle for the selective oxidation of methane to produce oxygenates [1,2], and was observed in situ for the CH_4–O_2–NO_x system at temperatures higher than 773 K [5]. The observation of HONO, which is formed from NO_2, suggests that, in agreement with the on-line results, NO_2 is the active catalyst in the CH_3OH–O_2–NO_x system.

4.4. Theoretical calculations

The above experimental results indicate that NO_2 may play a catalytic role in methanol oxidation. In order to understand the details of the mechanism, we employed quantum chemical methods to calculate the possible reaction pathways.

Table 2
Seven investigated channels in the hydrogen abstraction reactions of CH_3OH by NO_2

Channel	Reaction	Transition state
1	$CH_3OH + NO_2 \rightarrow CH_2OH + cis\text{-HONO}$	TS1
2	$CH_3OH + NO_2 \rightarrow CH_2OH + cis\text{-HONO}$	TS2
3	$CH_3OH + NO_2 \rightarrow CH_2OH + trans\text{-HONO}$	TS3
4	$CH_3OH + NO_2 \rightarrow CH_2OH + HNO_2$	TS4
5	$CH_3OH + NO_2 \rightarrow CH_3O + cis\text{-HONO}$	TS5
6	$CH_3OH + NO_2 \rightarrow CH_3O + trans\text{-HONO}$	TS6
7	$CH_3OH + NO_2 \rightarrow CH_3O + HNO_2$	TS7

In the initial step of methanol oxidation of the CH_3OH–O_2–NO (or CH_3OH–O_2–NO_2) co-feed system, five possible reactions involving CH_3OH decomposition can be deduced from chemical intuitions:

$$CH_3OH + O_2 \rightarrow CH_2OH + HO_2 \quad (3)$$

$$CH_3OH + NO \rightarrow CH_2OH + HNO \quad (4)$$

$$CH_3OH + NO \rightarrow CH_3O + HNO \quad (5)$$

$$CH_3OH + NO_2 \rightarrow CH_2OH + HONO\,(or HNO_2) \quad (6)$$

$$CH_3OH + NO_2 \rightarrow CH_3O + HONO\,(or HNO_2) \quad (7)$$

The experimental apparent activation energy for reaction (3) is 44.9 kcal mol^{-1} [21], and the experimental enthalpy changes for reactions (4)–(7) are 48.1, 54.4, 19.7 and 25.9 kcal mol^{-1}, respectively [22], indicating that reactions (6) and (7) are most possible initial steps for the hydrogen abstraction of methanol in the CH_3OH–O_2–NO_x system. Thus, in the following discus-

Table 3
Relative energies of all species calculated at the CBS-Q and B3LYP/6-311++G(2d,p) level[a]

Species	Relative energies at the B3LYP/6-311++G(2d,p) level	Relative energies at the CBS-Q level	Relative energies at the CCSD (T)/6-311++G(2d,p)//MP2/6-311++G(2d,p) level [25]
CH_3OH+NO_2	0	0	
TS1	18.9	20.5	
IMr1	−0.7	−2.5	
IMp1	15.3	13.9	
TS2	19.8	21.2	
IMr2	0.2	−2.3	
IMp2	16.1	14.9	
$CH_2OH + cis$-HONO	18.8	18.2	
TS3	24.8	27.0	
IMp3	15.0	11.7	
$CH_2OH + trans$-HONO	18.3	17.7	
TS4	20.8	24.1	28.4
IMp4	20.4	20.7	
$CH_2OH + HNO_2$	25.2	25.9	
TS5	21.9	32.7	
$CH_3O + cis$-HONO	24.6	27.8	
TS6	25.2	35.2	
$CH_3O + trans$-HONO	24.1	27.3	
TS7	25.5	34.9	40.8
IMp7	25.7	30.3	
$CH_3O + HNO_2$	31.0	35.5	

[a] ZPE (zero point energy) corrected energies, unit: kcal mol^{-1}.

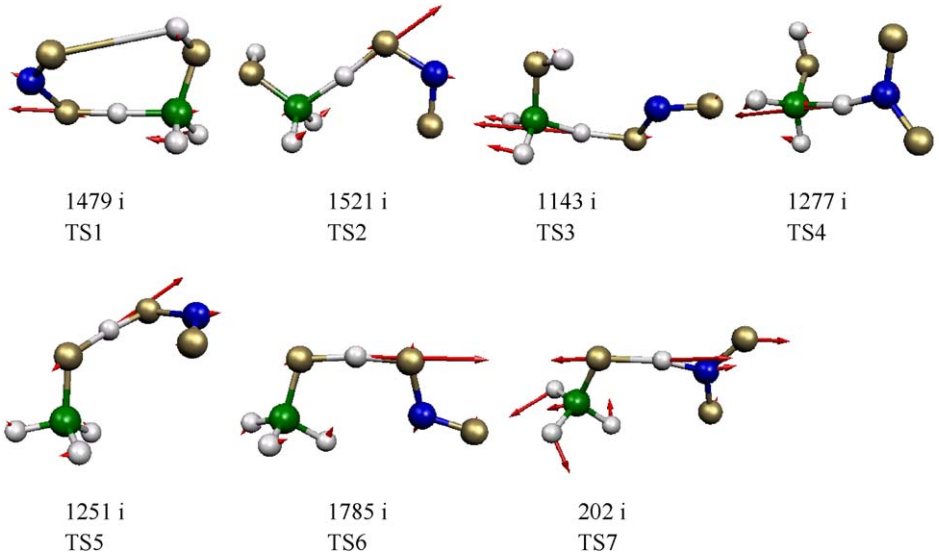

Fig. 8. Transition state geometries optimized at the B3LYP/6-311++G(2d,p) level. The corresponding imaginary frequencies are listed below. The arrows in each transition state denote the vibrational directions in the imaginary frequency mode.

sions we will focus on reactions (6) and (7), i.e., the reactions between methanol and nitrogen dioxide.

The reactions between methanol and nitrogen dioxide were investigated experimentally by Anastasi [23] and Koda [24], and theoretically by Tabata [25]. However, Anastasi and Koda only measured the overall reaction rates and obtained the activation energy of 21.4 kcal mol^{-1} [23]. Tabata and co-workers studied the enhancement effects of added methanol on methane-selective oxidation in the presence of NO_2 [25]. They calculated two channels (channels 4 and 7 in Tables 2 and 3) at the CCSD(T)//MP2/6-311++G(2d,p) level of theory. However, they neglected other channels (e.g. channels 1 and 2) whose activation energies may be lower than for channels 4 and 7. Their calculated activation energies (28.4 and 40.8 kcal mol^{-1}) are much higher than the experimental value of 21.4 kcal mol^{-1} [23]. Thus, further theoretical investigations are still desired.

Although NO_2 is a radical molecule, its first excited electronic state ($^2B_1$) lies above the ground state ($^2A_1$) by 42.9 kcal mol^{-1} [26], which is much higher than the experimental activation energy of 21.4 kcal mol^{-1}. Therefore, the reactions of methanol with excited states of NO_2 will not be concerned here.

4.4.1. Reaction mechanism, geometries and energy profile

Table 2 lists the seven possible channels investigated in the present study for the reactions of CH_3OH with NO_2. The optimized transition states for the seven channels are shown in Fig. 8 (the optimized geometries for other species are documented in the supporting materials). Table 3 gives the relative energies of

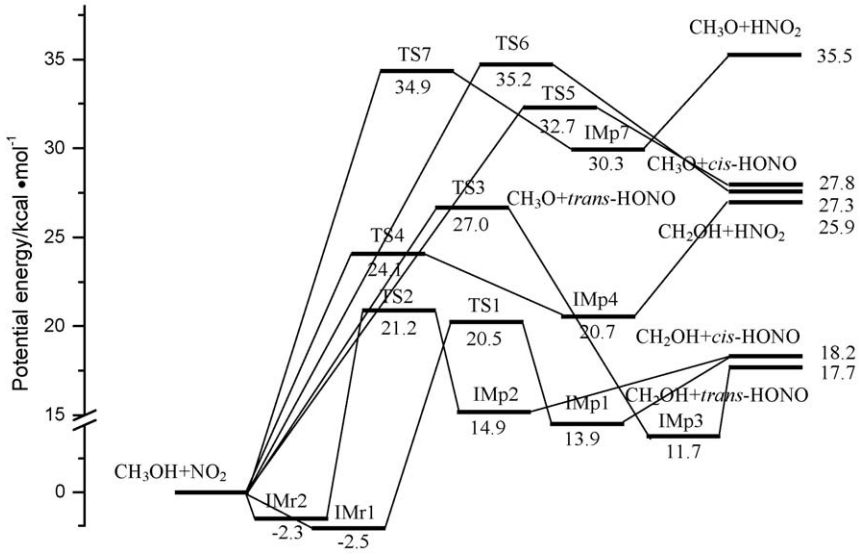

Fig. 9. Potential energy diagram of the CH_3OH and NO_2 reactions at the CBS-Q//B3LYP/6-311++G (2d,p) level.

all the species involved in the reactions and Fig. 9 shows the schematic energy profile of the reactions.

It is clear from Table 2 and Fig. 9 that CH_2OH is produced from channels 1–4 by abstracting a hydrogen atom from the methyl group and that CH_3O is produced from channels 5 to 7 by abstracting a hydrogen atom from the hydroxyl group. Both channels 1 and 2 produce *cis*-HONO + CH_2OH, the only difference between these two channels being the attacking orientation of NO_2 with respect to the OH group in CH_3OH (cf. TS1 and TS2 in Fig. 8). Channel 3 produces *trans*-HONO + CH_2OH whereas channel 4 produces HNO_2 + CH_2OH. Channels 5, 6 and 7 produce *cis*-HONO + CH_3O, *trans*-HONO + CH_3O and HNO_2 + CH_3O, respectively. Although some van der Waals complexes or hydrogen-bonded complexes exist for the reactants and products, all the seven channels can be treated as elementary reactions with a transition state for each.

First of all, we notice that the geometries of *cis*-HONO and *trans*-HONO are remarkably different. In *cis*-HONO, the bond length between the nitrogen atom and the hydroxyl oxygen atom is 1.392 Å, whereas this bond is 1.433 Å in *trans*-HONO. The geometrical difference between *cis*-HONO and *trans*-HONO is probably caused by the difference in the repulsion of the lone-pair electrons between the two oxygen atoms. In *trans*-HONO, this repulsion is stronger and makes the N–O bond longer than that of *cis*-HONO. The geometrical difference between *cis*-HONO and *trans*-HONO also has influence on the structures of the transition states that produce HONO + CH_2OH. In TS1 and TS2, which will form *cis*-HONO, the forming H–O bond length and breaking C–H bond length are 1.232 and 1.367 Å, and 1.221 and 1.379 Å, respectively. However, in TS3, which will form *trans*-HONO, the forming H–O bond length and breaking C–H bond length are 1.365 and 1.240 Å, respectively. Apparently, TS1 and TS2 look more similar to the reactants, but TS3 looks more similar to the products. The geometrical difference between the transition states yielding HONO + CH_3O is small. In TS5, which will form *cis*-HONO + CH_3O, the forming H–O bond length and breaking O–H bond length are, respectively, 1.131 and 1.299 Å, which are close to the corresponding bond lengths of 1.148 and 1.256 Å in TS6, which will form *trans*-HONO + CH_3O. For the two channels that form HNO_2, the forming H–N bond length and breaking C–H/O–H bond length of TS4 and TS7 are 1.209 and 1.490 Å, and 1.097 and 1.488 Å, respectively. It is clear that the forming bond lengths of the transition states in the HONO + CH_3O channels are shorter than those in the HONO + CH_2OH channels.

From Table 3 and Fig. 9 we can see that the barrier heights of all the channels forming CH_2OH are remarkably lower than those forming CH_3O; the largest barrier height (TS3, 27.0 kcal mol^{-1}) forming CH_2OH is by 5.7 kcal mol^{-1} lower than the lowest barrier height (TS5, 32.7 kcal mol^{-1}) forming CH_3O. Thus, the channels forming CH_2OH are more favored than the channels forming CH_3O. Among the channels forming CH_2OH, the barrier heights forming *cis*-HONO (TS1, 20.5 kcal mol^{-1}; TS2, 21.2 kcal mol^{-1}) are lower than those forming *trans*-HONO (TS3, 27.0 kcal mol^{-1}) and HNO_2 (TS4, 24.1 kcal mol^{-1}). In particular, the barrier heights forming *cis*-HONO are in good agreement with the experimental result of 21.4 kcal mol^{-1} [23]. The difference in the barrier heights between the channels forming *cis*-HONO and *trans*-HONO is probably due to the difference in the structures between *cis*-HONO and *trans*-HONO. These barrier heights indicate that only the two lowest channels are important at low temperatures since a difference of 1 kcal mol^{-1} in the barrier height will typically result in a factor of about 5 in the rate constants.

4.4.2. Rate constant calculations

The rate constants for channels 1–4 are calculated using μVT with Eckart tunneling corrections. The overall rate constants are also evaluated according to the rate constants of these channels. Since all the channels are elementary reactions and the forward reaction is the rate controlling reaction, the overall rate constants is simply the sum of the rate constants of each channel. The structural parameters employed in the rate constants calculations are given in Table 4. Fig. 10 displays the Arrhenius plots of the rate constants versus temperature. The fitted three-parameter forward and reverse rate constant expressions at 300–3000 K

Table 4
Some molecular and transition state parameters used for μVT rate constant calculations

Species	Energies (hartrees)[a]	I_i (amu)	Frequencies (cm^{-1})[b]
CH_3OH	−115.5867	14.1, 73.1, 75.8	289, 1038, 1076, 1169, 1368, 1477, 1495, 1507, 2993, 3040, 3110, 3841
NO_2	−204.8574	7.5, 138.3, 145.8	761, 1381, 1671
CH_2OH	−114.9216	9.3, 60.4, 69.1	415, 546, 1055, 1193, 1360, 1483, 3127, 3270, 3836
cis-HONO	−205.4908	21.2, 136.7, 157.9	631, 687, 874, 1338, 1697, 3590
trans-HONO	−205.4917	19.1, 143.9, 163.0	581, 616, 816, 1301, 1763, 3759
HNO_2	−205.4802	16.8, 137.0, 153.8	787, 1052, 1397, 1512, 1631, 3177
TS1	−320.4077	197.5, 626.7, 763.3	1479i, 83, 110, 173, 262, 417, 485, 624, 821, 1084, 1103, 1146, 1178, 1265, 1382, 1410, 1488, 1559, 3046, 3165, 3774
TS2	−320.4062	141.9, 845.7, 970.1	1520i, 34, 105, 184, 199, 375, 492, 580, 813, 1077, 1082, 1161, 1166, 1246, 1373, 1418, 1485, 1581, 3059, 3179, 3814
TS3	−320.3973	149.3, 753.3, 874.6	1143i, 87, 110, 186, 282, 394, 541, 636, 714, 941, 1099, 1153, 1206, 1333, 1391, 1452, 1511, 1603, 3023, 3151, 3749
TS4	−320.4026	184.9, 779.7, 915.3	1277i, 42, 56, 161, 293, 393, 456, 611, 815, 1085, 1115, 1182, 1281, 1375, 1396, 1479, 1529, 1616, 3056, 3185, 3807

[a] Without ZPE (zero point energy) corrections, calculated at the CBS-Q level by following formula: E(CBS-Q)-ZPE(B3LYP/6-311++G(2d,p)).
[b] Calculated at the B3LYP/6-311++G (2d,p) level.

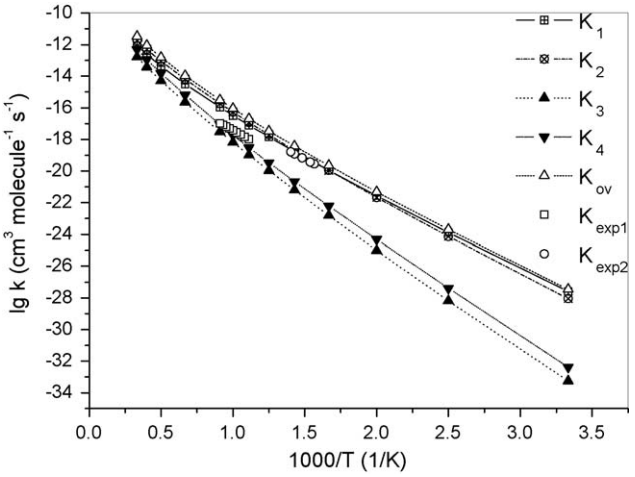

Fig. 10. Theoretical and experimental rate constants for the CH_3OH and NO_2 reactions. k_1, k_2, k_3, k_4: forward rate constants for channels 1, 2, 3 and 4, respectively; k_{ov}: calculated overall forward rate constant; k_{exp1}, k_{exp2}: experimental overall rate constants from Anastasi [23] and Koda [24], respectively. The theoretical rate constants were estimated by μVT/Eckart method.

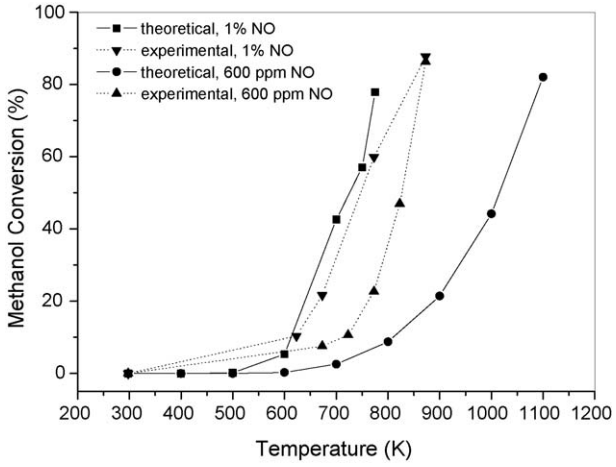

Fig. 11. Comparison of experimental (cf. Table 1) and theoretical methanol conversions of the CH_3OH–O_2–NO_x system.

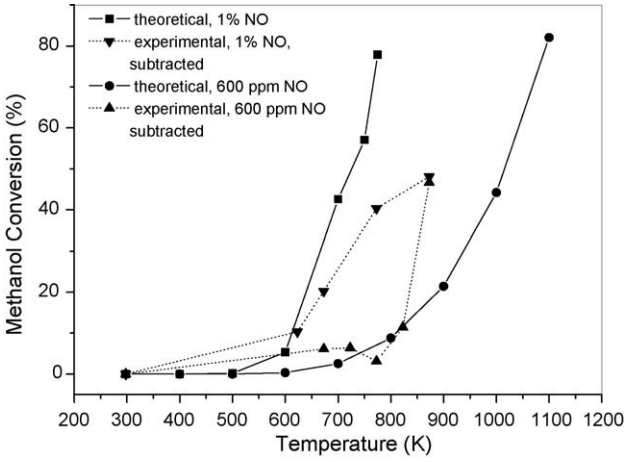

Fig. 12. Comparison of experimental (cf. Table 1) and theoretical methanol conversions of the CH_3OH–O_2–NO_x system. The spontaneous oxidation of methanol (i.e., in the absence of NO) was subtracted from the experimental value in the presence of NO.

for channels 1 to 4 are given in Table 5. We can see that the rate constants of channels 1 and 2 dominate almost over the whole temperature range. At 300–600 K, k_1 for channel 1 is the largest, whereas at 600–3000 K k_2 becomes the largest and about twice of k_1, indicating that channel 2 is predominant at high temperature. These results also show that channels 1 and 2 are the main reactions for hydrogen abstraction reactions of methanol by NO_2, yielding CH_2OH and *cis*-HONO as the main products. Since the rotational barrier for *cis*-HONO → *trans*-HONO isomerization is rather low (11.5 kcal mol^{-1}) [27], it is not surprising that both *cis*-HONO and *trans*-HONO can be observed with similar yields in the in situ infrared spectroscopy.

The calculated and experimental overall rate constants are also shown in Fig. 10. The recommended three-parameter fitting overall rate constant expression for this reaction is $1.72 \times 10^{-22} T^{3.38} \exp(-10153\,T^{-1})$ cm^3 molecule^{-1} s^{-1}. At 700 K, the overall rate constant is estimated at 3.76×10^{-19} cm^3 molecule^{-1} s^{-1}, which is close to the experimental data of 1.21×10^{-19} cm^3 molecule^{-1} s^{-1} obtained by Koda at 700 K [24]. However, at higher temperature, the divergence between calculated and experimental values becomes greater. This may be caused by a more complicated mechanism and deserves further studies.

4.5. Kinetic modelling of methanol conversion of the CH_3OH–O_2–NO_x system

Using the calculated rate constants and appropriate reaction conditions (CH_3OH 5%, N_2 balance, NO 1% or 600 ppm, flow rate 40 ml min^{-1}, reaction zone volume 8.2 ml, and the thermochemical data from ref. [33]), the methanol conversion of the

Table 5
Calculated μVT/Eckart rate constant expressions ($k = AT^n \exp(-E_a/RT)$, units: cm^3 molecule s J)

Channel	Forward rate paramerers			Reverse rate paramerers		
	A	n	E_a (J mol^{-1})	A	n	E_a (J mol^{-1})
Overall	1.72×10^{-22}	3.38	8.44×10^4	–	–	–
1	2.40×10^{-22}	3.17	8.46×10^4	3.94×10^{-24}	3.31	-1.79×10^3
2	6.71×10^{-22}	3.14	8.53×10^4	3.27×10^{-22}	2.90	6.79×10^3
3	3.71×10^{-23}	3.32	1.09×10^5	5.11×10^{-24}	3.20	2.93×10^4
4	4.01×10^{-21}	2.90	1.15×10^5	6.39×10^{-23}	3.28	2.26×10^3

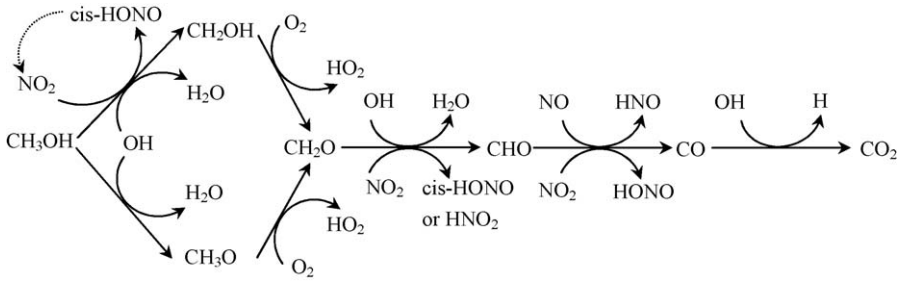

Fig. 13. Proposed overall reaction mechanism for the CH_3OH–O_2–NO_x system.

CH_3OH–O_2–NO_x system can be simulated by assuming the chemical equilibrium of reaction (2). The results are plotted in Fig. 11 in comparison with the experimental data (Table 1). It can be seen that, in the case of 1% NO, the simulated results are very close to the experimental values. In the case of 600 ppm of NO, the theoretical results deviate significantly from the experimental data. However, when the spontaneous oxidation of methanol is excluded from the experimental data, the agreement is much better, at least for low temperatures (see Fig. 12). Due to complicated reaction mechanisms, the good agreement between theory and experiment cannot be expected for high temperatures.

4.6. The overall reaction mechanism of the CH_3OH–O_2–NO_x system

Based on the present theoretical calculations and previous work, the overall reaction pathways can now be proposed for the CH_3OH–O_2–NO_x system (Fig. 13).

In the initial step, CH_3OH reacts with NO_2 to give CH_2OH and *cis*-HONO as the main products, i.e.,:

$$CH_3OH + NO_2 \rightarrow CH_2OH + \textit{cis}\text{-HONO} \quad (8)$$

It should be noted that this is different from the results obtained by Tabata [25].

It is well known that CH_2OH decomposes very easily in the presence of O_2 [28,29]:

$$CH_2OH + O_2 \rightarrow CH_2O + HO_2 \quad (9)$$

CH_2O may then react further with NO_2 to give HCO and *cis*-HONO or HNO_2 [4,21,29–31]:

$$CH_2O + NO_2 \rightarrow HCO + \textit{cis}\text{-HONO} \quad (10)$$

$$CH_2O + NO_2 \rightarrow HCO + HNO_2 \quad (11)$$

Carbon oxides are therefore finally produced from HCO [10,21,32].

An interesting issue is the recycling of NO_2. Indeed, there are several possible ways in which the intermediate species HONO (either *cis*- or *trans*-) may be converted to NO_2. For example, it may decompose to give NO directly through thermal dissociation [31,32] via reaction (12), or give NO_2 through the reaction with OH radical [32] or oxygen [34] via reactions (13) or (14). Furthermore, as mentioned before, NO readily reacts with molecular oxygen or HO_2 [28] to produce NO_2 (reactions (2) and (15)) and thus accomplish the NO_x recycling:

$$HONO + M \rightarrow NO + OH + M \quad (12)$$

$$HONO + OH \rightarrow NO_2 + H_2O \quad (13)$$

$$HONO + O_2 \rightarrow NO_2 + HO_2 \quad (14)$$

$$2NO + O_2 \rightarrow 2NO_2 \quad (2)$$

$$NO + HO_2 \rightarrow NO_2 + OH \quad (15)$$

It should be emphasized here that CH_2OH formed from reaction (8) is very active and may give OH radicals via reactions (9) and (15) [9]. The OH radical thus formed is also an excellent initiator for the activation of methanol:

$$CH_3OH + OH \rightarrow CH_2OH + H_2O \quad (16)$$

$$CH_3OH + OH \rightarrow CH_3O + H_2O \quad (17)$$

The activation energies for reactions (16) and (17) were reported to be 0.9 and 3.5 kcal mol^{-1}, respectively [35], implying that OH is very likely to accelerate the activation of methanol after the initiation of methanol via reaction (8). This aspect will be investigated in details in our further work.

5. Conclusions

In the absence of NO, the temperature required to initiate the deep oxidation of methanol is at least 773 K and the predominant product is carbon monoxide. In the presence of 600 ppm NO, the initial reaction temperature is reduced to 673 K while CO_2 becomes the predominant product. However, it is NO_2 that plays the catalytic role in the methanol oxidation process in the CH_3OH–O_2–NO_x system.

The reaction mechanism for the CH_3OH–O_2–NO_x system has been studied by both in situ IR and theoretical calculations. Methanol oxidation proceeds with the following sequence: $CH_3OH \rightarrow CH_2OH \rightarrow CH_2O \rightarrow HCO \rightarrow CO \rightarrow CO_2$. The initial step for methanol oxidation is: $CH_3OH + NO_2 \rightarrow$ TS1/TS2 $\rightarrow CH_2OH$ + *cis*-HONO. The calculated reaction barriers for the two lowest reaction channels are 20.5 and 21.2 kcal mol^{-1}, respectively, in good agreement with the experimental value of 21.4 kcal mol^{-1}. The overall rate constant obtained by the μVT calculations can be expressed as $1.72 \times 10^{-22} T^{3.38} \exp(-10153\ T^{-1})$ cm^3 $molecule^{-1}$ s^{-1}, from which a value of 3.76×10^{-19} cm^3 $molecule^{-1}$ s^{-1} can be

obtained for the temperature of 700 K, to be compared with the experimental value of 1.21×10^{-19} cm^3 molecule^{-1} s^{-1}. The μVT rate constant calculations have confirmed that channels 1 and 2 contribute mostly to the reactions of methanol and NO_2. The theoretically simulated methanol conversion of the CH_3OH–O_2–NO_x system is in satisfactory agreement with the experiment.

It is important to notice that NO_2-catalyzed deep oxidation of methanol has a significant adverse influence on the selective oxidation of methane catalyzed by NO_2, resulting in very low yields for methanol and related oxygenates. However, the deep oxidation is a significant benefit to the complete combustion of gasoline-based fuels containing methanol as additive. On the other hand, the deep oxidation of methanol catalyzed by NO_2 as demonstrated by this work may significantly disturb the overall reactions involved in the selective reduction of NO_x using methane as the reductant.

Acknowledgment

The research of this work was sponsored by the National Natural Science Foundation of China (Project Nos. 20273004, 20333020, 20473002, 20533010, 20573003 and 2006CB601103).

Appendix A. Supplementary data

Supplementary data associated with this article can be found, in the online version, at doi:10.1016/j.molcata.2006.02.064.

References

[1] K. Tabata, Y. Teng, Y. Yamaguchi, H. Sakurai, E. Suzuki, J. Phys. Chem. A 104 (2000) 2648.
[2] K. Otsuka, R. Takahashi, I. Yamanaka, J. Catal. 185 (1999) 182.
[3] M.A. Bañares, J.H. Cardoso, G.J. Hutchings, J.M.C. Bueno, J.L.G. Fierro, Catal. Lett. 56 (1998) 149.
[4] J.A. Barbero, M.C. Alvarez, M.A. Bañares, M.A. Peña, J.L.G. Fierro, Chem. Commun. (2002) 1184.
[5] Z. Yan, C.-X. Xiao, Y. Kou, Catal. Lett. 85 (2003) 135.
[6] Z. Yan, C.-X. Xiao, Y. Kou, Catal. Lett. 85 (2003) 129.
[7] C.-X. Xiao, Z. Yan, Y. Kou, J. Nat. Gas Chem. (China) 12 (2003) 90.
[8] I. Kenichi, T. Yano, Bull. JSME 26 (1983) 211.
[9] M.D. Fokema, J.Y. Ying, Catal. Rev. 43 (2001) 1.
[10] P. Taylor, L. Cheng, B. Dellinger, Combust. Flame 115 (1998) 561.
[11] M.U. Alzueta, R. Bilbao, M. Finestra, Energy Fuels 15 (2001) 724.
[12] Gaussian 98, Revision A.7, M.J. Frisch, G.W. Trucks, H.B. Schlegel, G.E. Scuseria, M.A. Robb, J.R. Cheeseman, V.G. Zakrzewski, J.A. Montgomery, Jr., R.E. Stratmann, J.C. Burant, S. Dapprich, J.M. Millam, A.D. Daniels, K.N. Kudin, M.C. Strain, O. Farkas, J. Tomasi, V. Barone, M. Cossi, R. Cammi, B. Mennucci, C. Pomelli, C. Adamo, S. Clifford, J. Ochterski, G.A. Petersson, P.Y. Ayala, Q. Cui, K. Morokuma, D.K. Malick, A.D. Rabuck, K. Raghavachari, J.B. Foresman, J. Cioslowski, J.V. Ortiz, A.G. Baboul, B.B. Stefanov, G. Liu, A. Liashenko, P. Piskorz, I. Komaromi, R. Gomperts, R.L. Martin, D.J. Fox, T. Keith, M.A. Al-Laham, C.Y. Peng, A. Nanayakkara, C. Gonzalez, M. Challacombe, P.M.W. Gill, B. Johnson, W. Chen, M.W. Wong, J.L. Andres, C. Gonzalez, M. Head-Gordon, E.S. Replogle, J.A. Pople, Gaussian, Inc., Pittsburgh PA, 1998.
[13] A.D. Becke, J. Chem. Phys. 98 (1993) 5648.
[14] C. Lee, W. Yang, R.G. Parr, Phys. Rev. B 37 (1988) 785.
[15] B. Miehlich, A. Savin, H. Stoll, H. Preuss, Chem. Phys. Lett. 157 (1989) 200.
[16] J.W. Ochterski, G.A. Petersson, J.A. Montgomery Jr., J. Chem. Phys. 104 (1996) 2598.
[17] Shaowen Zhang, Thanh N. Truong, VKLab Version 1.0, University of Utah, 2001.
[18] S.A. Anderson, T.W. Root, J. Catal. 217 (2003) 396–405.
[19] J.-M. Tatibouët, H. Lauron-Pernot, J. Mol. Catal. A: Chem. 171 (2001) 205.
[20] Turnover frequency = [(mole of product produced)/(mole of added catalysts)] per second.
[21] J.H. Bromly, F.J. Barnes, S. Muris, X. You, B.S. Haynes, Combust. Sci. Tech. 115 (1996) 259.
[22] Experimental data derived, from NIST webbook (http://webbook.nist.gov/).
[23] C. Anastasi, D.U. Hancock, J. Chem. Soc. Faraday Trans. 284 (1988) 1697.
[24] S. Koda, M. Tanaka, Combust. Sci. Technol. 47 (1986) 165.
[25] Y. Teng, Y. Yamaguchi, T. Takemoto, K. Tabata, E. Suzuki, Phys. Chem. Chem. Phys. 2 (2000) 3429.
[26] G. Herzberg, Molecular Spectra and Molecular Structure, D. Van Nostrand Company, INC., vol. 3, 1966, p. 602.
[27] G.R. De Maré, Y. Moussaoui, Int. Rev. Phys. Chem. 18 (1999) 91.
[28] C.K. Westbrook, F.L. Dryer, Combust. Sci. Tech. 20 (1979) 125.
[29] P. Glarborg, M.U. Alzueta, K. Dam-Johansen, Combust. Flame 115 (1998) 1.
[30] Z.F. Xu, M.C. Lin, Int. J. Chem. Kinet. 35 (2003) 184.
[31] M.U. Alzueta, J.M. Hernández, Energy Fuels 16 (2002) 166.
[32] T. Faravelli, A. Frassoldati, E. Ranzi, Combust. Flame (2003) 188.
[33] I. Barin, Thermochemical Data of Pure Substances, VCH, New York, USA, 1993.
[34] P. Glarborg, M.U. Alzueta, K. Kjærgaard, K. Dam-Johansen, Combust. Flame 132 (2003) 629.
[35] J.T. Jodkowski, M.-T. Rayez, J.-C. Rayez, J. Phys. Chem. A 103 (1999) 3750.